Environ Fluid Mech (2009) 9:509–523
DOI 10.1007/s10652-009-9127-6

ORIGINAL ARTICLE

Evaluating the dimensionality and significance of "active periods" in turbulent environmental flows defined using Lipshitz/Hölder regularity

Christopher J. Keylock

Received: 9 December 2008 / Accepted: 4 March 2009 / Published online: 18 March 2009

Abstract Active periods within perturbed boundary-layer flows are considered in terms of the local roughness of measured velocity time series and defined in terms of Hölder/Lipshitz exponents. Such events are associated with the passage of energetic, coherent flow structures and are responsible for exerting high turbulent stresses because of the rapid changes in velocity that occur at such times. A method is proposed for assessing the effective dimensionality of such active periods, as well as their significance to the flow field, for a particular choice of flow metric. The method is applied to the turbulent flow through a confluence flow geometry, with velocity samples acquired close to the bed of the channel in a zone of complex mixing. The dimensionality of the active periods is consistent with the observed patterns of sediment entrainment from the bed, with the significance of the active periods decaying away from the erosional zone.

Keywords Hölder/Lipschitz regularity · Roughness exponents · Intermittency · Flow dimensionality · River confluences

1 Introduction

Although turbulence is inherently three-dimensional, approximating the flow field by models of reduced dimensionality is often sufficient in various fields, including the transport of scalars in forests [11], or the study of rotating flows approximated by shallow-water theory (as suggested by Taylor-Proudman theory) [2,6,34]. In addition, two-dimensional turbulence is of interest in its own right [13,14,34]. One field where a two-dimensional approximation is often made is in the study of erosion and transport of particles from the bed of perturbed boundary-layer flows (e.g. the study of aeolian sediment transport [28], blowing snow [29] or sediment transport in water flows [4,10,27]). In this case, a vertical coordinate (z) combined with a coordinate in the longitudinal direction (x) can be used to study the relation between

C. J. Keylock (✉)
School of Geography, University of Leeds, Woodhouse Lane, Leeds, UK
e-mail: c.j.keylock@leeds.ac.uk

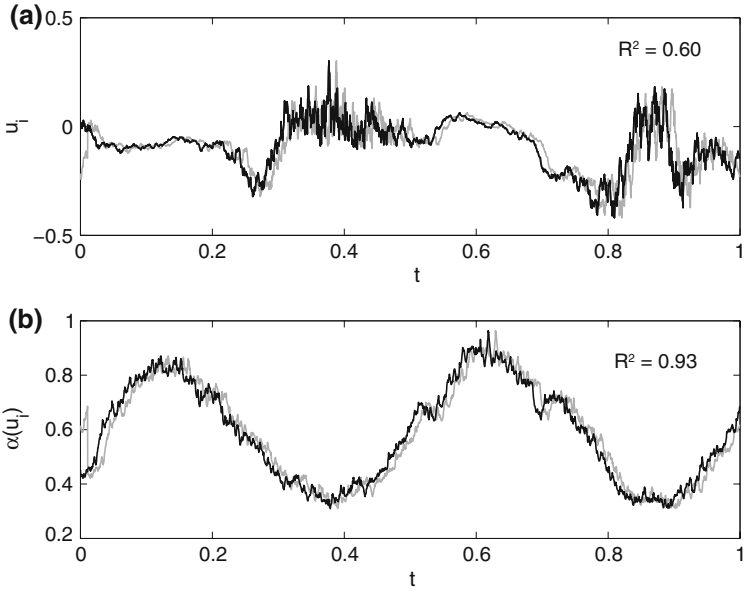

Fig. 1 Two example, intermittent, velocity signals are shown in **a** in black and gray, together with their coefficient of determination (R^2). The data in (**b**) are the corresponding roughness measures (α)

sediment entrainment and the x–z component of the Reynolds stress, or by considering individual quadrant [7] contributions to the Reynolds stress [26] and their relation to sediment transport [10,27,38]. This assumes that the transverse velocity component in the y direction makes a minimal contribution to the sediment entrainment process.

Perhaps the simplest approach to assessing the effective dimensionality of the flow is through a comparison of the variances of the different velocity components. Cross-correlative or cross-spectral analyses will also permit an assessment of the degree of coherence at particular frequencies, on average. However, the aim of this paper is to consider the effective dimensionality of the active periods within the flow, defined as those times when the local roughness of the velocity signals is high [18], i.e. they fluctuate greatly. Hence, we are examining the dimensionality of the dynamically important periods rather than the whole flow field. The intermittent nature of turbulence [24] results in an inherent variability to the fluctuations of turbulence velocity data, which is compounded in environmental boundary layers by wake shedding, Kelvin-Helmholtz instabilities and similar processes leading to the occasional passage of particularly energetic flow structures. It is these periods that are generally of greatest interest for characterising flow mixing, turbulent stresses or sediment entrainment, and it is the dimensionality of these that is isolated and investigated here.

Figure 1a shows two hypothetical, intermittent velocity series, u_i, in black and gray. While they are clearly correlated, the time scale of fluctuations in the flow is relatively short, meaning that the coefficient of determination (R^2) between the two signals is not that high. However, what is perhaps even clearer in this figure is that the periods when the flow is relatively rough and smooth are closely related. Using a measure of signal roughness, α, explained in Sect. 2, Fig. 1b shows that the correlation between these roughness measures is much higher. The method introduced in [18] used these α-series to delimit active periods in the flow, defined in an n-dimensional sense as the times when $n\alpha$-series were simultaneously less than average.

For the data in Fig. 1b, the two series fulfil this condition 47% of the time, but such periods account for 67% of $\left|u_1' u_2'\right|$, where the prime indicates a fluctuating quantity. Furthermore, such periods contain virtually all of the high frequency energy in the signal.

The aim of this paper is to consider a method for defining the dimensionality of these active flow periods. The first part of Sect. 2 briefly introduces the notion of Hölder/Lipschitz regularity and a practical method of calculating the Hölder exponent time series for a particular velocity time series. For three orthogonal velocity components it is then possible to formulate 7 criteria for an active period based on the consideration of each velocity component individually, each pair of components, and the three components simultaneously. In addition, the complement to this definition is given by the times that are not considered to be an active period. A statistic is formulated given a choice of an appropriate flow measure (e.g. turbulence intensity) that compares the average value for this measure between the active periods and their complement. A means of placing confidence intervals on this statistic is outlined using surrogate data methods. The most effective definition of an active period for capturing the greatest variability of the flow statistic defines the effective dimensionality of the flow. If the observed value for the statistic is not significantly different to appropriately developed null models from surrogate data, then active periods are not significant to the flow dynamics, indicating that few energetic flow structures are present and, hence, that the defined active periods are not dynamically important relative to general fluctuations about the mean velocity.

While methods such as Particle Imaging Velocimetry (PIV) and related holographic methods are increasingly used in experimental turbulence studies [1,30,37], the method presented in this paper is developed for the case of single-point velocity measurements in an Eulerian frame—the most typical situation for field campaigns in environmental turbulence, that is still used for precise measurement of turbulence statistics in experimental flows [35]. The method is applied to three-dimensional velocity time series measured using a field instrument in a hydraulic flume, where the sampling resolution is sufficient to capture the dominant scales of coherent structures.

2 Dimensionality criteria

2.1 Lipshitz/Hölder regularity

An active period for a velocity component i was considered to occur by [18] when the local roughness of the velocity signal was high. Consequently, an active period over velocity components i and j, or i, j and k was the intersection of active periods on the individual components. This analysis was built around the calculation of pointwise Hölder/Lipshitz exponents, α, for the time series of orthogonal velocity components. These were shown to have both a simpler cross-correlation structure than the velocity data that was also less sensitive to coordinate rotation, as well as isolating periods in the flow that accounted for a higher proportion of $\sum \left|u_i' u_j'\right|$ or $\sum \left|u_i' u_j' u_k'\right|$ than quadrant-based methods, or even those based on $\left|u_i' u_j' u_k'\right|$ or $\left|u_i' u_j'\right|$ directly. Delimiting active periods in flows based on Hölder/Lipshitz regularity is logical given the (simplified) view of turbulence as a multifractal process [24,25]. Because a non-singular support for a fractal signal implies that multifractality is present, the roughness of the signal will vary through time. Isolating the rougher periods in the flow across multiple velocity components provides an intuitive measure of the periods when the flow is in a relatively active state.

Hölder/Lipshitz exponents characterise the regularity of a function at a point and their study is underpinned mathematically by the work of Littlewood and Paley [23], and research on the regularity of functions in Banach and Sobolev function spaces, which can also be employed for studying the Navier–Stokes equations directly [8,9]. The Hölder exponent can be thought of as related to the fractal dimension of the function at that point. Thus, for a unidimensional time-series, with fractal dimension, D_f, bounded by the integers 1 and 2, the pointwise Hölder regularity is $2 - D_f$. More formally, we consider the differentiability of a signal (its smoothness) relative to polynomial approximations within the local domain of a specific point. Hence, if we study a velocity series, $u(t)$, in a neighbourhood, δ about a position, T, then from a Taylor series expansion:

$$p_T(t) = \sum_{i=0}^{m-1} \frac{u^i(T)}{i!} (t - T)^i \tag{1}$$

where m is the number of times that u is differentiable in $T \pm \delta$. Defining the approximation to $u(t)$ at T by $p_T(t)$ as

$$\varepsilon_T(t) = u(t) - p_T(t) \tag{2}$$

then the order of differentiability of $u(t)$ close to T gives an upper bound on $\varepsilon_T(t)$:

$$|\varepsilon_T(t)| \leq \frac{|t - T|^m}{m!} \tag{3}$$

This upper bound is then given by a non-integer Hölder/Lipshitz exponent, where a function $u(t)$ has a pointwise Hölder exponent, $\alpha_u \geq 0$ if a constant $K > 0$ and the polynomial $p_T(t)$ of degree m exist such that

$$|u(t) - p_T(t)| \leq K |t - T|^\beta \tag{4}$$

The Hölder regularity, $\alpha(u)$, of $u(t)$ at T is then given by the supremum of β that fulfil (4).

Accurate estimation of Hölder exponents can be undertaken in appropriate function spaces constructed for this purpose [21], or via refinements to the work of [23] on wavelet bases [12]. However, a simple and rapid method was used by [18] that gave good results based on a log–log regression of the signal oscillations, $O_{T\pm\delta}$, within some distance δ of T against δ, where $O_{T\pm\delta}$ is given by:

$$O_{T\pm\delta} = \max\left(u_{t\in(T-\delta,\ldots T+\delta)}\right) - \min\left(u_{t\in(T-\delta,\ldots T+\delta)}\right) \tag{5}$$

and δ is distributed logarithmically (from 2^1 to 2^{10} in this study). This and other methods for calculating Hölder exponents are available in the *Fraclab* toolbox (http://apis.saclay.inria.fr/FracLab/).

2.2 The effective dimensionality of the flow

Figure 2 shows a 40 s segment of velocity time series measured in three perpendicular dimensions from the experiment in a hydraulic flume described in Sect. 3. Three orthogonal velocity components are shown where coordinate subscripts 1, 2 and 3 correspond to the longitudinal (x), transverse (y) and vertical (z) directions. The mean-subtracted, fluctuating velocity components are shown as indicated by the prime. In addition, Fig. 2d gives the fluctuating α series for each velocity component, i, through time (the dependence of α_i' on t is assumed and

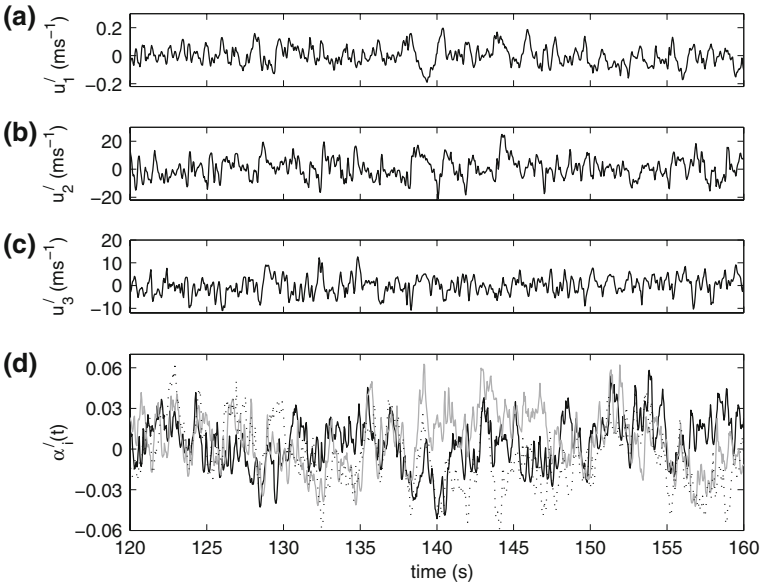

Fig. 2 Fluctuating velocity time series for three orthogonal velocity components (**a**–**c**), along with their corresponding, fluctuating Hölder series (**d**). The black line in (**d**) is for α_1', the black, dotted line is for α_2' and the gray line is for α_3'

removed for notational convenience in what follows). These forty seconds of data are visualised in Fig. 3 using a wavelet visualization method due to [17]. Consideration of three velocity components necessitates a movement away from two-dimensional quadrants [7,10,27] to the definition of flow octants:

$$\begin{aligned}
\text{octant } +1 &\in \left\{u_1' > 0, u_2' > 0, u_3' > 0\right\} \\
\text{octant } -1 &\in \left\{u_1' > 0, u_2' < 0, u_3' > 0\right\} \\
\text{octant } +2 &\in \left\{u_1' < 0, u_2' > 0, u_3' > 0\right\} \\
\text{octant } -2 &\in \left\{u_1' < 0, u_2' < 0, u_3' > 0\right\} \\
\text{octant } +3 &\in \left\{u_1' < 0, u_2' > 0, u_3' < 0\right\} \\
\text{octant } -3 &\in \left\{u_1' < 0, u_2' < 0, u_3' < 0\right\} \\
\text{octant } +4 &\in \left\{u_1' > 0, u_2' > 0, u_3' < 0\right\} \\
\text{octant } -4 &\in \left\{u_1' > 0, u_2' > 0, u_3' < 0\right\}
\end{aligned} \tag{6}$$

Defining a flow event as a period of time when the threshold hole size, H, is exceeded, where this threshold is defined by the product of the standard deviations, σ:

$$\left|u_1' u_2' u_3'\right| > H\sigma(u_1)\,\sigma(u_2)\,\sigma(u_3) \tag{7}$$

then Fig. 3 highlights all events exceeding $H = 1$ during this 40 s period. The wavelet decompositions of the velocity data suggest that the vertical components is the least important contributor to the individual events, with the highest contribution from a single velocity component being from u_1 at 138–139 s at wavelet scale 5. However, the large contributions at low frequencies (high wavelet scales) across both u_1 and u_2 at 143.8 and 144.3 s suggest that at these times there is a particularly large contribution to the Reynolds stress in the longitudinal-transverse plane by −4 and +4 octants. These two time periods are shown in Fig. 2 to have very different characteristics, with all $\alpha_i' < 0$ from 138.0 s to 138.5 s, suggesting a

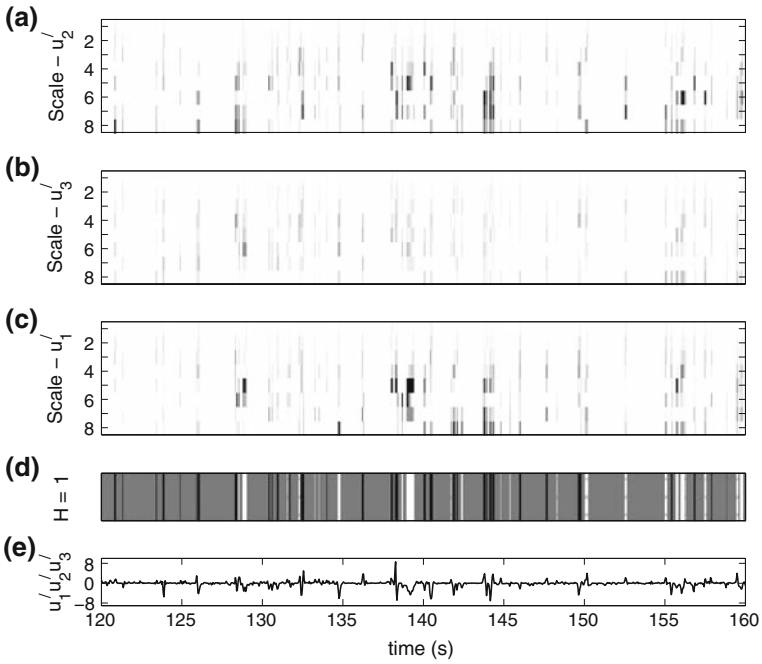

Fig. 3 A wavelet decomposition of the 40 s of data from Fig. 2 highlighting the presence of different octant turbulence structures in the record. These plots are described more completely in [16], and employ an undecimated wavelet transform to highlight the scales that contribute most greatly to particular octant events. The normalisation of the wavelet coefficients is undertaken over all scales and all velocity components for a direct comparison of the shading. The value for the wavelet scales increases with increasing width of the wavelet filter (decreasing frequency). The velocity triple product is given in (**e**), while (**d**) shows the identified octants (Eq. 6) for a hole size, H, of 1.0. Against a background of medium gray, quadrant 2 events are white, quadrant 4 events are black, quadrant 1 events are dark gray and quadrant 3 events are light gray. Cross-hatching indicates that the octant designation is negative ($u'_2 < 0$)

three-dimensional flow structure, but with only $\alpha'_2 < 0$ at 144 s suggesting that this term is dominant (which is supported qualitatively by the darker shading for u'_2 at this time in Fig. 3).

Thus, given some measure of the flow, the effective dimensionality of an active period at some point in time, T, can be defined as the number of velocity components for which $\alpha_i < H_\alpha$ that maximise the value for the flow measure, where H_α is some threshold condition that may be constant across all velocity components or a function of the velocity component under consideration. In this paper we consider perhaps the simplest choice for H_α:

$$H_a(i) = \bar{\alpha}_i \tag{8}$$

which equates to $\alpha'_i = 0$.

2.3 Measures of effective dimensionality

A summary measure for the whole time series is required to determine the average effective dimensionality of the active periods, although it is acknowledged that this may change with time due to the passage of different flow structures with varying characteristics as noted in Sect. 2.2. In fact, and with greater generality, what is required is a particular approach to formulating such a measure as the specific metric that one wishes to employ may depend on

the purpose of the research undertaken as well as the number of velocity components available for analysis. In this study, we assume that the metrics (M) most likely to be of interest are the three pairwise (unsigned) covariances, the unsigned triple product and the turbulence intensity, given respectively as:

$$M_{ij} = \left|u_i' u_j'\right| \tag{9a}$$

$$M_{123} = \left|u_1' u_2' u_3'\right| \tag{9b}$$

$$M_{123+} = \sqrt{\left(u_1'\right)^2 + \left(u_2'\right)^2 + \left(u_3'\right)^2} \tag{9c}$$

Flow dimensionality (G) can be assessed by isolating those periods that exceed the Hölder exponent threshold in one, two or three-dimensions:

$$G_i \in \{\alpha_i < H_\alpha(i)\} \tag{10a}$$

$$G_{ij} \in \{\alpha_i < H_\alpha(i)\} \cap \left\{\alpha_j < H_\alpha(j)\right\} \tag{10b}$$

$$G_{123} \in \{\alpha_1 < H_\alpha(1)\} \cap \{\alpha_2 < H_\alpha(2)\} \cap \{\alpha_3 < H_\alpha(3)\} \tag{10c}$$

If the complement of these sets is also formed, e.g. $G_i^C \notin \{\alpha_i < H_\alpha(i)\}$, then the average value for the metric M over the set G and its complement may be used to evaluate the effective dimensionality of the flow. An appropriate statistic in this case is

$$S = \frac{\overline{M(G)} - \overline{M\left(G^C\right)}}{\overline{M(G)} + \overline{M\left(G^C\right)}} \tag{11}$$

where M is a chosen metric and G is a flow dimensionality criterion and the overbar indicates some form of average.

2.4 Confidence limits on the measures

Because a non-zero value for (11) could arise by chance, it is useful to place confidence limits on these measures. This we do by following the surrogate data generation philosophy [36] commonly employed in nonlinear physics. For example, phase synchronisation measures are generally compared to the mean phase synchronisation for several random sorts of the phase data [22], while intermittency and structures in turbulent flows have been evaluated using surrogates that preserve both the histogram of the original data and its spectral properties [3,31]. The computation of such surrogates can be undertaken using Fourier [32] or wavelet-based methods [15,16,19]. Given the simple nature of the null hypothesis in this study, the Fourier method (known as the Iterated Amplitude Adjusted Fourier Transform, or IAAFT method) was adopted.

Figure 4 shows the velocity and Hölder series for 40 s of data as well as an IAAFT surrogate series. Because the IAAFT algorithm is applied to each velocity component separately, with no cross-spectral characteristic preserved except by chance, the surrogate series provide a null hypothesis result for the methods described in Sect. 2.3. For example, for calculations over the full 300 s of data for the time series in Fig. 4, using M_{123+}, with all seven possibilities for G compared, the three-dimensional measure of flow dimensionality G_{123} has the highest value for S (Fig. 5a), suggesting that the flow is fully three-dimensional at this location. However, the surrogates also exhibit an increase for G_{123}, and in terms of the number of standard deviations of the surrogates that separates the mean of the surrogates from the value for the data, either the transverse velocity component or the transverse and vertical components

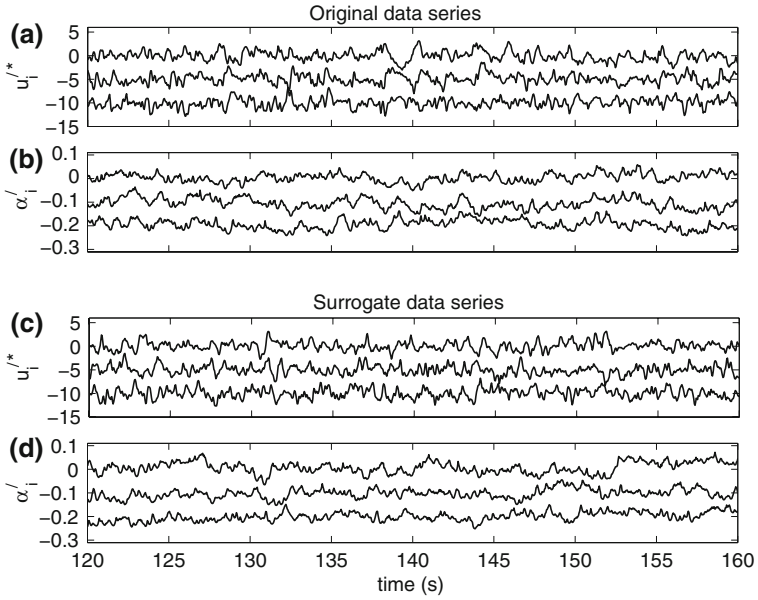

Fig. 4 The velocity data from Fig. 2 are given in (**a**) normalised by their standard deviation ($u_i'^*$) and displaced vertically for clarity ($u_1'^*$ by 0; $u_2'^*$ by -5; $u_3'^*$ by -10), along with their α_i' series in (**b**), displaced vertically by 0 for α_1', -0.1 for α_2', and -0.2 for α_3'. The equivalent results for a set of IAAFT surrogate data are given in (**c**) and (**d**)

in combination appear to define the flow dimensionality. In contrast, further downstream (Fig. 5b), the relative importance of the longitudinal velocity component increases and the dimensionality is fully three-dimensional, with the most important contribution coming from the combined longitudinal-transverse components.

It is to be emphasised that our approach based on the active periods in the flow is different to standard approaches based on the velocity variance ratios or cross-spectra and focuses more upon the flow topology as the active periods, dominated by energetic flow structures are extracted and considered relative to the background flow. As such, our approach acts as a complement to traditional methods. For example, based on the ratio of standard deviations, both datasets in Fig. 5 would be considered fully three-dimensional because $\sigma(u_1)/\sigma(u_2) = 0.91$ and 1.00 for the datasets in Fig. 5a,b, respectively, while $\sigma(u_1)/\sigma(u_3) = 1.62$ and 1.87, respectively.

3 The dimensionality measures in practice

The data studied so far in this study were obtained in a hydraulic flume using an acoustic Doppler velocimeter recording three perpendicular components at 25 Hz. Data were obtained for 300 s from a sampling volume with its base 1 median grain size ($\sim$2.5 mm) above a fixed bed (sediment glued into position) in the post-confluence region of a parallel-channel confluence, an experimental configuration used by [5] to study the effects of vortex interactions at river channel confluences (as opposed to incorporating momentum effects that occur with junction angles >0°). The hydraulic flume had a width of 305 mm and a 9 mm splitter plate

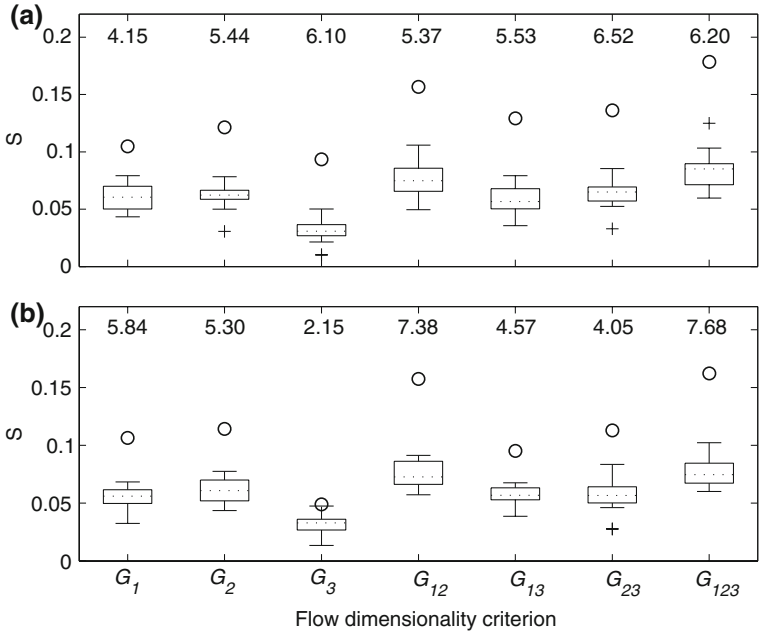

Fig. 5 The results for calculating the flow dimensionality using turbulence intensity, M_{123+}, for the full 300 s of data illustrated in Figs. 1, 2 and 3 over all measures G for the metric S (circles) is given in (**a**), with results for an alternative flow location in (**b**). The results for surrogate series are given as a boxplot in each case (*dotted line* is the median; the box delimits the upper and lower quartiles; whiskers extend for up to 1.5 times the interquartile range from these quartiles; outliers are shown by *crosses*). The numbers across the top of each plot indicate the number of standard deviations that the values for S for the data are separated from the mean of the surrogates

was placed along the centre of the flume to partition the two flows, one of which passed over a step with a height, H, of 50 mm. The flow depth in the raised channel was 70 mm and 120 mm in the unraised channel, with flow velocities of 0.55ms^{-1} and 0.52ms^{-1}, respectively, meaning that the Reynolds number in both channels exceeded 35,000 and the Froude number was less than 0.45. Flow structures in this flow configuration are more complex than the three scales of turbulence seen in a backward-facing step flow (individual Kelvin–Helmholtz vortices shed from the step in the x–z plane; flapping of the shear layer's position; periodic breakdown of the shear layer) [33], through the introduction of vortex shedding in the x–y plane from the splitter plate that interacts in a complex fashion with these other scales, which modelling studies have shown depends on the channel width [20].

Figure 6 shows a view from above of applying such a flow to a fully mobile bed for 1 h, with the location of various sampling locations superimposed, illustrating that the sample locations capture the regions where flow structures exert the greatest stresses. The data in Figs. 2, 3, 4 and 5a are from ($x/H = 5$, $y/F = 0.23$), while the data in Fig. 5b are from ($x/H = 6$, $y/F = 0.23$). Over one hour, virtually no erosion has taken place downstream of the channel without a step ($y/F > 0.5$) or for $x/H < 3.0$ (which is within the flow recirculation zone downstream of the step for $y/F < 0.5$). Vortex impingement associated with structures generated at the shear layer that delimits the recirculation zone can be seen from $3.0 < x/H < 5.5$, with deposition at $y/F < 0.15$ and $x/H > 5.0$. The velocity spectra in Fig. 7 (estimated using the multitaper method) show that the peak in frequency within the region of vortex impingement on the bed is at ∼1 Hz, which is well within the

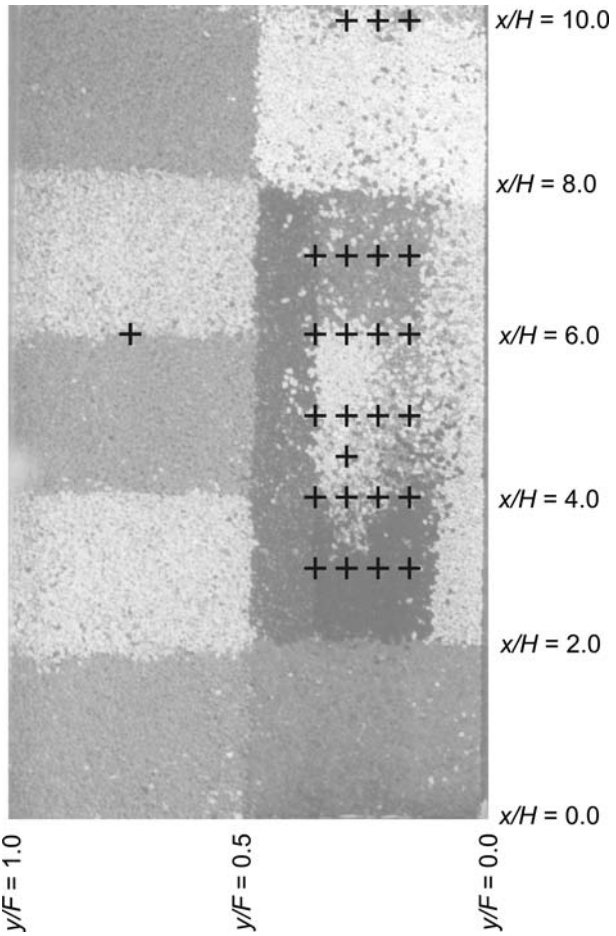

Fig. 6 The post-confluence region for a parallel-channel confluence flow after one hour of erosion of a mobile bed. Sediment movement is restricted to locations where flow structures generated by the step (positioned between $y/F = 0$ and $y/F = 0.5$) interact with those from the vertical splitter plate at $y/F = 0.5$ (where F indicates the flume width). The crosses are the sampling locations where velocity data were collected over a fixed bed

Nyqvist cut-off of 12.5 Hz for the instrument used and is sampled adequately by a 300 s time series duration.

Figures 8 and 9 give results for three longitudinal transects and one transverse transect based on metrics M_{123} and M_{123+}. The ordinate, S_{surr} indicates that the statistic S from (11) has been re-expressed in terms of the mean and standard deviation of the surrogate data, S_*, according to:

$$S_{surr} = \frac{S - \overline{S_*}}{\sigma\,(S_*)} \tag{12}$$

The seven different definitions of flow dimensionality, G, based on different combinations of the α-series for various velocity components are shown by different symbols. The dotted line at $S_{surr} = 1.96$ corresponds to a 2.5% significance level for a one-tailed test, if it is assumed

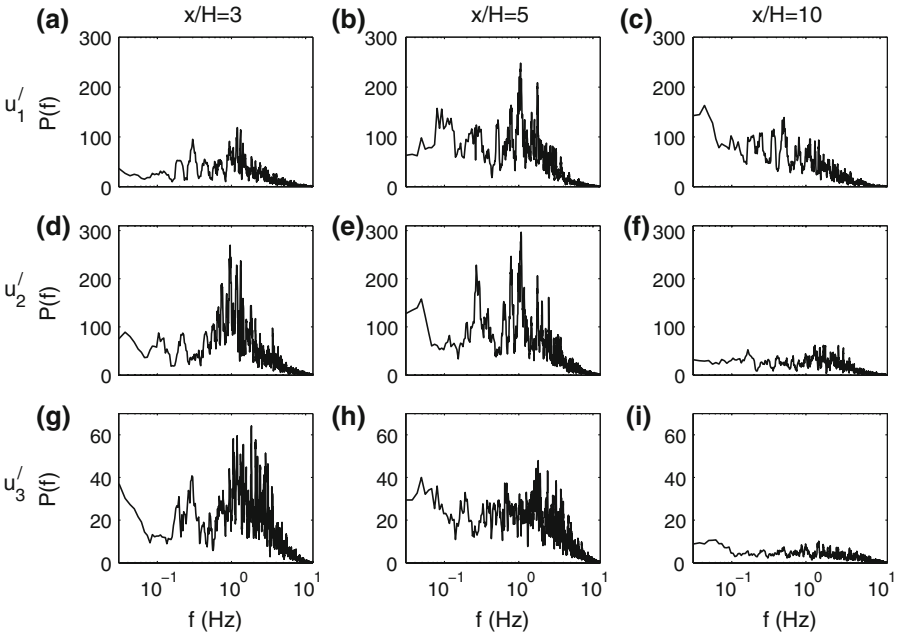

Fig. 7 The power spectral density for the three velocity components as a function of *x/H* at $y/F = 0.23$. Note the change in scale for the vertical velocity component (**g**), (**h**) and (**i**)

that the surrogates are normally distributed. It is clear that by $x/H = 10$ (Fig. 8) and for $y/F > 0.5$ (Fig. 9), the dimensionality measures are generally not significant. This indicates that coherent flow structures are either decaying or no longer present at these locations and, consequently, that values for M_{123} or M_{123+} are not particularly associated with any choice of G. The spectra in Fig. 7 show the decline in energy at $x/H = 10$, which diminishes the change in α_i relative to background variability.

For this experiment, with the possible exception of ($x/H = 6.0$, $y/F = 0.23$) measured using M_{123+} (Fig. 9b) rather than M_{123} (Fig. 9a), full three-dimensionality of the active periods is not discerned. Instead, at ($x/H = 6.0$, $y/F = 0.16, 0.23$) the high values for G_{12} and the barely significant values for G_3 show that the active periods at these locations are organised in the *x*–*y* plane. However, closer to the step, i.e. ($x/H = 4$, $y/F = 0.16, 0.23$), where eddy impingement upon the bed is clear from Fig. 6, Fig. 8a,b show that the dimensionality of the active periods is in the *y*–*z* plane (gray triangles are dominant). Closer to the step and within the flow recirculation zone at ($x/H = 3$, $y/F = 0.16$), Fig. 8a shows that G_2 gives the most significant result, but that results in general are less significant at this position than they are for $x/H = 3$ and $y/F = 0.23, 0.30$. In particular, Fig. 8c shows that all choices for G give highly significant results at ($x/H = 3$, $y/F = 0.30$), which can be explained by the fact that this point lies close to, but beyond, the mean reattachment position and is affected by both flapping of the mean reattachment location [33], and lateral draw-in of fluid into the recirculation zone formed behind the step from the deeper flow at $y/F > 0.5$. The complexity of this flow environment is highlighted at $x/H = 5$, where at $y/F = 0.30$ the dimensionality of the active periods is dominated by the vertical and vertical-transverse components (Fig. 8c), while at $y/F = 0.16$ (4 cm away), these are the least important terms.

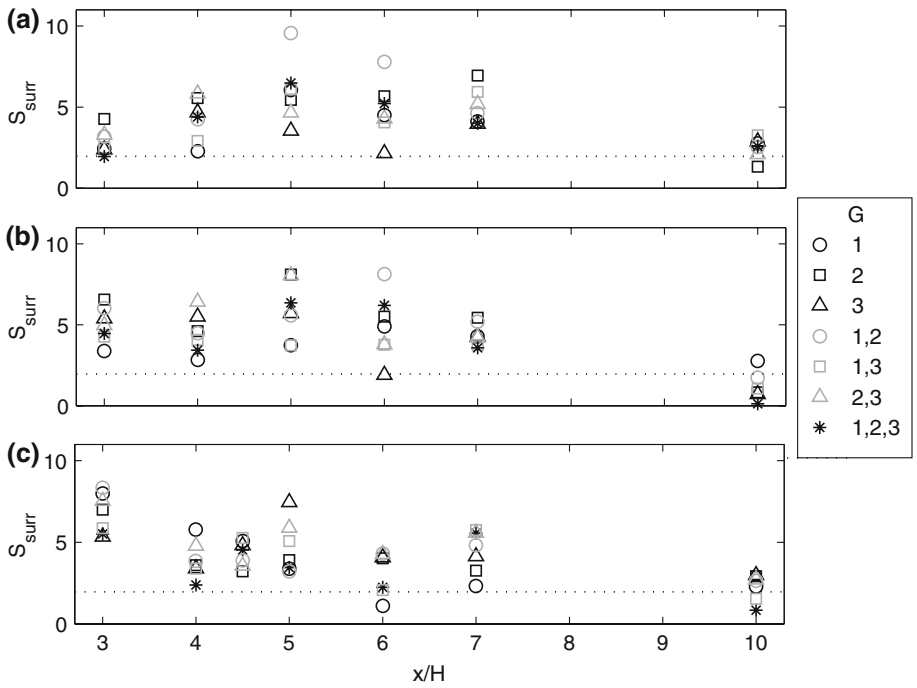

Fig. 8 Three longitudinal transects of S_{surr} for metric M_{123} at $y/F = 0.16$ (**a**), $y/F = 0.23$ (**b**) and $y/F = 0.30$ (**c**). The seven possible definitions for G (Fig. 5) are given by different symbols as indicated in the legend. The *dotted line* corresponds to 1.96 standard deviations from the mean

The general interpretation that for $x/H < 6$ (or $x/H < 5$ at $y/F = 0.16$) the active periods have an important vertical component (Fig. 8), but that at $x/H = 6$ (Fig. 9a), the x–y component is most important, is consistent with the erosion map in Fig. 6. Rapid accelerations and decelerations about a grain of sediment on the bed that have a vertical component, and are coherent with fluctuations in another plane will exert high forces promoting entrainment. If the dimensionality of the structures shifts to the longitudinal-transverse plane, then high lateral stresses may cause the sediment grain to pivot in its position, potentially making it easier to erode the sediment by a subsequent flow event, and they may also transport particles already eroded. However, the lack of an important vertical component to such active periods reduces the potential for sediment entrainment. Hence, consideration of the dimensionality of the active periods and their significance relative to null surrogate data, leads to an understanding of the flow topology that is consistent with observed patterns of sediment entrainment.

4 Conclusion

In this paper a method has been presented for determining the effective dimensionality of the active periods in a turbulent flow. These are defined in terms of the Hölder/Lipshitz regularity of the orthogonal velocity components measured at one position. Having calculated these exponents for each velocity time series using Eq. 5, the active periods are given by the intersection over the velocity components of those periods where roughness is greater than

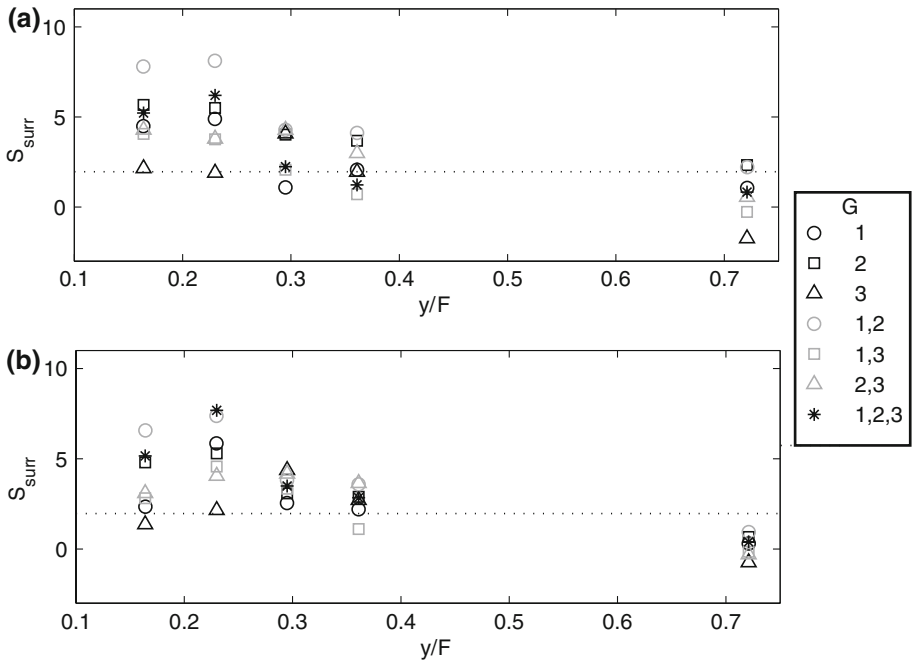

Fig. 9 A transverse transect of S_{surr} at $x/H = 6.0$ for metric M_{123} (**a**), and M_{123+} (**b**). The seven possible definitions for G (Fig. 5) are given by different symbols as indicated in the legend. The *dotted line* corresponds to 1.96 standard deviations from the mean

average (Hölder regularity is less than average). Having identified these active periods and an appropriate measure of the flow characteristics for a particular study (e.g. the turbulence intensity, Eq. 9c), a simple statistic is formulated comparing the average value of this measure for those periods classified as active periods and those that are not (Eq. 11). To interpret the value from Eq. 11 in terms of a confidence interval, surrogate velocity series are generated from the original data that preserve the original histogram and linear structure (autocorrelation), but randomise the nonlinear parts (the Hölder regularity). Consequently, Eq. (12) gives the significance of the measure on the data relative to the linear surrogates. By choosing to define an active period in a variety of ways (Eq. 10), diagrams such as Fig. 8 permit the dimensionality of these active periods to be established.

This new approach is potentially of use to a wide range of studies of environmental turbulent flows, where understanding the nature of the flow structures that constitute the active flow periods and their contribution to turbulence intensity or Reynolds stresses is important. This includes studies of mixing, pollutant dispersal, estimation of gaseous fluxes (e.g. CO_2 emissions from forests [31]), and sediment transport. The Eulerian approach taken to flow structure identification in this paper also makes the method broadly applicable to field-based study. Further work is required on the optimal choice of threshold in Eq. (8) for identifying active periods that correspond to particular flow structures. In the future, a combined PIV and conventional velocity probe study in a wind tunnel or hydraulic flume will be undertaken to provide more guidance on this choice.

Acknowledgements The data in this paper were obtained while the author was in receipt of NERC Studentship GT04/97/55/FS.

References

1. Barnhart DH, Adrian RJ, Papen GC (1994) Phase-conjugate holographic system for high-resolution particle-image velocimetry. Appl Opt 33(30):7159–7170
2. Baroud CN, Plapp BB, Swinney HL, She ZS (2003) Scaling in three-dimensional and quasi-two-dimensional rotating turbulent flows. Phys Fluids 15(8):2091–2104. doi:10.1063/1.1577120
3. Basu S, Foufoula-Georgiou E, Lashermes B, Arneodo A (2007) Estimating intermittency exponent in neutrally stratified atmospheric surface layer flows: a robust framework based on magnitude cumulant and surrogate analyses. Phys Fluids 19(11):115102. doi:10.1063/1.2786001
4. Best J (2005) The fluid dynamics of river dunes: a review and some future research directions. J Geophys Res 110(F04S02). doi:10.1029/2004JF000218
5. Best JL, Roy AG (1991) Mixing layer distortion at the confluence of channels of different depth. Nature 350:411–413. doi:10.1038/350411a0
6. Boer GJ, Shepherd TG (1983) Large-scale two-dimensional turbulence in the atmosphere. J Atmos Sci 40(1):164–184. doi:10.1175/1520-0469(1983)040<0164:LSTDTI>2.0.CO;2
7. Bogard DG, Tiederman WG (1986) Burst detection with single-point velocity measurements. J Fluid Mech 162:389–413. doi:10.1017/S0022112086002094
8. Cannone M, Karch G (2005) About the regularized Navier–Stokes equations. J Math Fluid Mech 7:1–28. doi:10.1007/s00021-004-0105-y
9. Cannone M, Meyer Y (1995) Littlewood–Paley decomposition and the Navier–Stokes equations. Methods Appl Anal 2:307–319
10. Heathershaw AD, Thorne PD (1985) Sea-bed noises reveal role of turbulent bursting phenomenon in sediment transport by tidal currents. Nature 316(6026):339–342. doi:10.1038/316339a0
11. Hsieh CI, Siqueira M, Katul G, Chu CR (2003) Predicting scalar source-sink and flux distributions within a forest canopy using a 2-D Lagrangian stochastic dispersion model. Boundary-Layer Meteorol 109(2):113–138. doi:10.1023/A:1025461906331
12. Jaffard S (1991) Pointwise smoothness, two-microlocalization and wavelet coefficients. Publ Mater 35:155–168
13. Jimenez J, Moffatt HK, Vasco C (1996) The structure of vortices in freely-decaying two-dimensional turbulence. J Fluid Mech 313:209–222. doi:10.1017/S0022112096002182
14. Kevlahan NKR, Farge M (1997) Vorticity filaments in two-dimensional turbulence: creation, stability and effect. J Fluid Mech 346:49–76. doi:10.1017/S0022112097006113
15. Keylock CJ (2006) Constrained surrogate time series with preservation of the mean and variance structure. Phys Rev E Stat Nonlin Soft Matter Phys 73:036707. doi:10.1103/PhysRevE.73.036707
16. Keylock CJ (2007) A wavelet-based method for surogate data generation. Physica D 225:219–228. doi:10.1016/j.physd.2006.10.012
17. Keylock CJ (2007) The visualization of turbulence data using a wavelet-based method. Earth Surf Process Landf 32(4):637–647. doi:10.1002/esp.1423
18. Keylock CJ (2008) A criterion for delimiting active periods within turbulent flows. Geophys Res Lett 35:L11804. doi:10.1029/2008GL033858
19. Keylock CJ (2008) Improved preservation of autocorrelative structure in surrogate data using an initial wavelet step. Nonlinear Process Geophys 15:435–444
20. Keylock CJ, Hardy RJ, Parsons DR, Ferguson RI, Lane SN, Richards KS (2005) The theoretical foundations and potential for large-eddy simulation (LES) in fluvial geomorphic and sedimentological research. Earth Sci Rev 71(3–4):271–304. doi:10.1016/j.earscirev.2005.03.001
21. Kolwankar KM, Lévy Vehel J (2002) A time domain characterisation of the fine local regularity of functions. J Fourier Anal Appl 8:319–334. doi:10.1007/s00041-002-0016-3
22. Kreuz T, Mormann F, Andrzejak RG, Kraskov A, Lehnertz K, Grassberger P (2007) Measuring synchronization in coupled model systems: a comparison of different approaches. Physica D 225:29–42. doi:10.1016/j.physd.2006.09.039
23. Littlewood JE, Paley REAC (1936) Theorems on Fourier series and power series (II). Proc Lond Math Soc 42:52–89. doi:10.1112/plms/s2-42.1.52
24. Meneveau C, Sreenivasan KR (1991) The multifractal nature of turbulent energy-dissipation. J Fluid Mech 224:429–484. doi:10.1017/S0022112091001830
25. Muzy JF, Bacry E, Arneodo A (1991) Wavelets and multifractal formalism for singular signals—application to turbulence data. Phys Rev Lett 67(25):3515–3518 . doi:10.1103/PhysRevLett.67.3515
26. Nakagawa H, Nezu I (1977) Prediction of the contributions to the Reynolds stress from bursting events in open-channel flows. J Fluid Mech 80:99–128. doi:10.1017/S0022112077001554
27. Nelson JM, Shreve RL, McLean SR, Drake TG (1995) Role of near-bed turbulence structure in bed load transport and bed laod mechanics. Water Resour Res 31(8):2071–2086. doi:10.1029/95WR00976

28. Neuman CM, Lancaster N, Nickling WG (2000) The effect of unsteady winds on sediment transport on the stoss slope of a transverse dune, Silver Peak, NV, USA. Sedimentology 47(1):211–226. doi:10.1046/j.1365-3091.2000.00289.x
29. Nishimura K, Nemoto M (2005) Blowing snow at Mizuho station, Antarctica. Phil Trans R Soc A 363(1832):1647–1662
30. Noguchi K, Nezu I, Sanjou M (2008) Turbulence structure and fluid—particle interaction in sediment-laden flows over developing sand dunes. Environ Fluid Mech. doi:10.1007/s10652-008-9114-3
31. Poggi D, Porporato A, Ridolfi L, Albertson JD, Katul GG (2004) Interaction between large and small scales in the canopy sublayer. Geophys Res Lett 31(L05102). doi:10.1029/2003GL018611
32. Schreiber T, Schmitz A (1996) Improved surrogate data for nonlinearity tests. Phys Rev Lett 77:635–638. doi:10.1103/PhysRevLett.77.635
33. Simpson RL (1989) Turbulent boundary layer separation. Annu Rev Fluid Mech 21:205–234. doi:10.1146/annurev.fl.21.010189.001225
34. Speziale CG (1981) Some interesting properties of two-dimensional turbulence. Phys Fluids 24(8):1425–1427. doi:10.1063/1.863560
35. Staicu A, Mazzi B, Vassilicos JC, van de Water W (2003) Turbulent wakes of fractal objects. Phys Rev E Stat Nonlin Soft Matter Phys 67(6):066306. doi:10.1103/PhysRevE.67.066306
36. Theiler J, Eubank S, Longtin A, Galdrikian B, Farmer JD (1992) Testing for nonlinearity in time-series—the method of surrogate data. Physica D 58:77–94. doi:10.1016/0167-2789(92)90102-S
37. Westerweel J (1997) Fundamentals of digital particle image velocimetry. Meas Sci Technol 8(12):1379–1392. doi:10.1088/0957-0233/8/12/002
38. Wu F-C, Jiang M-R (2007) Numerical investigation of the role of turbulent bursting in sediment entrainment. J Hydraul Eng 133(3):329–334. doi:10.1061/(ASCE)0733-9429(2007)133:3(329)